A New Method to Measure Oxygen Surface Exchange Kinetics On Porous Mixed Conducting Oxides With Simple Determination of Microstructure Parameters

Clement Nicollet, Clement Meyssonnier, Simon Guillonneau, Alexandre Merieau, Insaf Abdouli

A new method to measure oxygen surface exchange kinetics on porous mixed conducting oxides with simple determination of microstructure parameters.

Clement Nicollet*, Clement Meyssonnier, Simon Guillonneau, Alexandre Merieau, Insaf Abdouli

Nantes Université, CNRS, Institut des Matériaux de Nantes Jean Rouxel, IMN, F-44000 Nantes, France
** Corresponding author: clement.nicollet@cnrs-imn.fr*

Abstract

Oxygen exchange reaction on mixed conducting oxide is a critical reaction for many applications, yet measuring its rate constant remains poorly reliable by standard techniques. Here, we propose a new technique that adapts the conductivity relaxation measurements on porous ceramics. Using a simple image analysis tool, it is possible to accurately determine the grain size distribution of the porous ceramic, which is used in a new relaxation model that integrates relaxation times over that distribution. With such model, it is possible to fit relaxation transients with the oxygen exchange reaction rate constant k_{chem} as the only fitting parameter. With such rigidity, the output values of k_{chem} are not sensitive to the fitting procedure, which does not require optimization. The model is proven to be applicable on various mixed conducting oxides and on a wide range of microstructures, yielding a remarkably low residual for each of the porous ceramics considered. The procedure is using porous ceramics, therefore the derived kinetics are representative of ceramics used in real applications such as fuel cells, sensors, or catalysis.

Graphical Abstract:

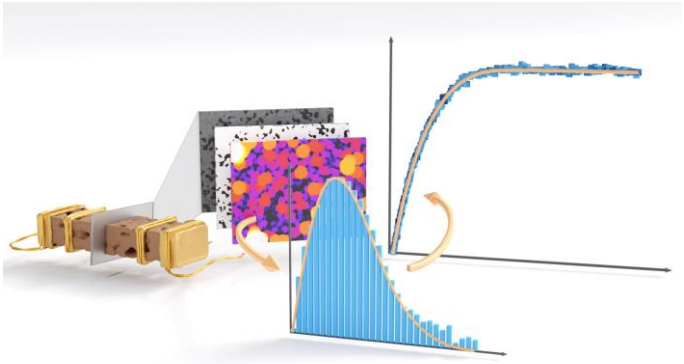

1 Introduction

The reaction of molecular oxygen on the surface of metal oxides with mixed ionic and electronic conductivity is critical for devices such as steam electrolyzers, solar fuels systems, permeation membranes, gas sensors, *etc.*[1–5]. The reaction can be a reduction of molecular oxygen and incorporation of an oxide ion into the lattice of the oxide, or an oxidation of the oxide ion and release of molecular oxygen in the gas phase. At the equilibrium, both reactions are equivalent and their overall kinetics are closely related, to the degree that they are often treated as one general reaction known as the oxygen exchange reaction. Despite the importance of this reaction in practical applications, the measurement strategies for studying its kinetics are poorly reliable. As a result, there is a wide spread of values for oxygen surface exchange coefficients in the literature, even for a given material. One possible reason for this spread is that some measurements of the oxygen surface exchange are only a collateral of measuring bulk oxygen diffusion in mixed conducting oxides. Indeed, to be able to treat the diffusion

problem analytically, the solution of the 2nd Fick's law requires a boundary condition that sets the concentration of oxide ions at the surface. This is usually done by introducing a reaction coefficient *k*, which defines the flux of oxide ions entering the material such that the boundary condition of the diffusion equation is set. Then, the Fick's second law of diffusion is solved with an analytical solution including both a diffusion coefficient *D* and a reaction coefficient *k*. The major drawback of this approach is that the determination of *k* is sensitive to how much the diffusion problem is affected by the boundary conditions. If the boundary condition is stable, meaning that the concentration of oxide ion at the surface is high enough not to influence the diffusion, then the determination of the surface reaction kinetics with diffusion based methods is inaccurate. Moreover, because the oxygen exchange reaction depends heavily on external parameters such as temperature and pressure, the level of accuracy for determining *k* depends on the measurement conditions. Then, conducting complete studies over wide ranges of measurements conditions inevitably introduces uncertainties in the results. For accurate determination of *k* values, it appears necessary to move away from techniques involving bulk diffusion and to develop protocols that are sensitive exclusively to oxygen surface exchange. In this endeavor, it is possible to modify the measurements procedures of classical techniques to render them essentially diffusion independent, thus enabling accurate determination of *k*.

A well-established measurement of *D* and *k* is the electrical conductivity relaxation experiment. Conductivity relaxation is based on the direct link that exists between the electrical conductivity of a mixed conducting oxide and its oxygen stoichiometry. As the stoichiometry of oxygen is at equilibrium with molecular oxygen in the gas phase, an abrupt change of oxygen partial pressure will trigger a change of oxygen stoichiometry in the material to equilibrate to the new oxygen pressure. The transient regime is controlled by the rate of oxygen surface exchange and bulk diffusion of the material. The change of oxygen stoichiometry can be monitored by conductivity measurements; the relaxation measurement is completed when the conductivity reaches a new stable value[6]. In the classical experiment, the sample is a dense ceramic; the transient is affected by the chemical diffusion coefficient D_{chem} and the chemical surface exchange coefficient of oxygen k_{chem}[7], which results in the determination of the latter being unreliable[8,9]. To render this technique more sensitive to surface exchange kinetics, it is, in principle, possible to reduce the dimensions of the samples to a thickness below a critical length L_c defined as $L_c = D_{chem}/k_{chem}$. However, reducing the sample dimensions below this critical length is not practical, because L_c is usually in the range of microns to hundreds of microns. Alternatively, the community has resorted to measuring dense thin films prepared by physical vapor deposition techniques such as pulsed laser deposition. The advantage is that the thickness of the films is well below the critical length, which makes them ideal for measuring k_{chem}. However, because their surface is small (1 cm^2), the derived k_{chem} lacks statistical accuracy. Additionally, because the surface is exposed, the films are very sensitive to airborne dust impurities, poisoning from handling, *etc.* therefore requiring a perfectly controlled lab environment and experimental procedure.

A less explored alternative to decrease the sample geometry under the critical length is to measure porous samples. In this case, the relevant diffusion length (that should be lower than L_c) is the distance between the gas phase to the bulk of the solid phase, *e.g.* the grain radius of the porous structure. The potential advantage of this approach is that the surface on which the reaction occurs is orders of magnitude higher than that of thin films, making the response more accurate. The second advantage is that most of the surface is inside the porous structure, therefore protecting it more to external pollutions than thin films. Originally, Ganeshanathan and Virkar described the strategy in an original paper, developing all considerations to perform conductivity relaxation on porous ceramics[10]. However, the exchange coefficients that were derived from these measurements were questionable. In our opinion, their measurements were done in conditions where the oxygen exchange kinetics were too fast, meaning that the transients were only limited by the time it takes to change the oxygen pressure in the measurement chamber, *e.g.* the flush time.

Although their derived k_{chem} were unsatisfying, the theoretical groundwork served us in an earlier work to prove the technique usable in the case of porous Pr-doped ceria ceramics, yielding plausible values for k_{chem} for this material[11]. In this case, the measurements conditions were set to temperatures low enough so that the flush time was fast compared to the oxygen exchange kinetics.

Recently, Zhang *et al.* have proposed an adaptation of the conductivity relaxation model to account for flush time and gas diffusion when measuring porous ceramics[12]. In their approach, the transients are fitted with a distribution of relaxation times, which allows discriminating features related to gas diffusion or surface exchange reaction[13,14]. Although the approach is interesting, we believe that fitting with a distribution of relaxation time would relieve too many degrees of freedom for the fit, which makes it less accurate for the determination of the oxygen surface exchange coefficient alone. Another concern comes from inability to accurately account for the microstructure. In all previous works cited above, the microstructure is simply described by two parameters, namely the specific surface area and the porosity. While in some cases this is sufficient[11], the model is too simple for most porous ceramics and does not yield accurate fits of the experimental data. Moreover, measuring surface area accurately can be challenging. For example, nitrogen adsorption measurements and BET theory can be poorly reliable for low surface areas, which would typically require large amounts of sample and are usually more suited for powders. Alternatively, 3D reconstruction of microstructures from Focused Ion Beam-Scanning Electron Microscopy (FIB-SEM) stacked images can be expensive and time consuming. Therefore, a new development that better account for the microstructure and that is easily accessible with common lab tools is required.

The measurement of oxygen surface exchange coefficients on porous ceramics has the potential to become a state-of-the-art measurement technique, if it can be proven to address two main concerns that currently limit the validity of the technique:

- Accounting for gas diffusion
- Accounting for microstructure

To this end, we are proposing an adaptation of the conductivity relaxation method to porous ceramics, with a focus on addressing these two main concerns. A new analytical model is developped, that accounts for both gas diffusion and microstructure while only using k_{chem} as fitting parameter. Additionally, we show a new experimental procedure to accurately determine representative microstructural parameters from simple microscopy images.

2 Theory

2.1 Accounting for microstructure

In a mixed conducting oxide at equilibrium with the oxygen pressure in the gas phase, the flux of oxygen entering or leaving the solid phase can be described with a simple first order reaction such as

$$\frac{1}{2}O_2 + v_O^{\cdot\cdot} + 2e' \rightleftharpoons O_O^x \qquad 1$$

For which the rate equation is

$$\frac{d[O_O^x]}{dt} = k_{chem}([O_O^x]_t - [O_O^x]_\infty) \qquad 2$$

Where $\frac{d[O_O^x]}{dt}$ is the flux of oxygen, k_{chem} is the rate constant or exchange coefficient, and $[O_O^x]_t$ and $[O_O^x]_\infty$ are the concentrations of oxygen in the solid phase at *t* and after equilibrium is reached. If the driving force leading this flux is of chemical nature, for example a change of oxygen chemical potential in the gas phase (a partial pressure step), the rate constant is called a chemical exchange coefficient k_{chem}[15]. When the dimension between the gas phase and the center of the solid phase is small compared to the

critical length L_c, the concentration of oxygen in the solid is homogeneous and k_{chem} is the only parameter that is needed to interpret the relaxation profiles.

After integration of the first order reaction rate expression, the evolution of the oxygen concentration as a function of time can be written as

$$g(t) = \frac{[O_O^x]_t - [O_O^x]_0}{[O_O^x]_\infty - [O_O^x]_0} = 1 - \exp\left(-\frac{t}{\tau}\right) \quad 3$$

In which $g(t)$ is the normalized concentration of oxygen in the solid phase, and τ is the time constant of the reaction. The time constant is a function of the rate constant k_{chem} and of the samples dimensions, namely its surface area A, and volume V, such as

$$\tau = \frac{V}{A \cdot k_{chem}} \quad 4$$

For a porous ceramic, the form factor V/A can be defined in various ways. In all previous work, and as introduced by Ganeshanathan and Virkar[10], the form factor is defined macroscopically: the volume is the apparent density of the solid phase, and the surface is the specific surface area of the ceramic. This yields:

$$\tau = \frac{1 - p}{S_A \cdot k_{chem}} \quad 5$$

With p the porosity of the sample and S_A the specific surface area.

Although a macroscopic form factor can be satisfactory in some cases (like in our previous work), it relies on the assumption that the microstructure is homogeneous such that all parts of the porous ceramic will equilibrate at the same rate. This implies that the grain size distribution of the ceramic is narrow and can be approximated to a single, mean grain diameter. In practice, obtaining such narrow distribution of grain sizes when preparing sintered ceramic is tedious and time consuming. Instead of using a macroscopic form factor, the microstructure of a sintered porous ceramic can be approximated by an array of cylinders, as it has been discussed previously by Lu *et al.*[16]. In this case, the form factor can be defined by the volume to area ratio of a cylinder such as

$$\frac{V}{A} = \frac{\pi \cdot R^2 \cdot L}{2 \cdot \pi \cdot R \cdot L} = \frac{R}{2} \quad 6$$

in which R is the radius and L is the length of the cylinders. The relaxation expression when considering cylinders becomes:

$$g(t) = 1 - \exp\left(-\frac{2 \cdot k_{chem}}{R} \cdot t\right) \quad 7$$

Using such "microscopic" definition of the form factor enables the introduction of heterogeneity in the microstructure. Indeed, if the cylinders are of different diameters, then the total relaxation becomes a sum of the relaxation of each cylinder, weighed by their probability density, such as

$$g(t) = 1 - \sum_n A_n \cdot \exp\left(-\frac{2 \cdot k_{chem}}{R_n} \cdot t\right) \quad 8$$

Where A_n is the probability of having a cylinder of a radius R_n. In this case, the total sum of A_n should be unity, which means that the probability density must be normalized for the model to be correct.

If the size distribution of the cylinders is determined *a priori*, and follows an analytic distribution function, then the expression of the relaxation can be integrated over the distribution function, and the expression becomes

$$g(t) = 1 - \int_0^{\infty} f(R_n) \cdot \exp\left(-\frac{2 \cdot k_{chem}}{R_n} \cdot t\right) \mathrm{d}R_n \qquad 9$$

In which $f(R_n)$ is the probability density function of the cylinders radii, which should also be normalized so that $\int_0^{\infty} f(R_n) \cdot dR_n = 1$.

With such expression, it should be possible to fully account for microstructure heterogeneity in the sample, which answers the first concern that arose when considering measurement of conductivity relaxation on porous ceramics. However, the model would only be accurate if the time constant associated to the step change of oxygen partial pressure is negligibly small compared to the relaxation of the oxygen stoichiometry. For faster relaxation rates, the second concern, namely gas diffusion, has to be taken into account.

2.2 Accounting for gas diffusion

As the relaxation technique relies on a step change of oxygen pressure in the gas phase, the speed at which the step change happens is of particular importance for the reliability of the technique. For dense samples, the only parameter affecting the step change is the geometry of the measurement chamber. As developed by Den Otter *et al.*[17], if the measurement chamber is considered as a continuously ideally stirred tank reactor, the normalized step change of pO_2 can be written as

$$\bar{p}(t) = \frac{p(t) - p_{\infty}}{p_0 - p_{\infty}} = \exp\left(-\frac{t}{\tau_{flush}}\right) \qquad 10$$

In which the time constant associated to the flush time is

$$\tau_{flush} = \frac{V_r}{F_{tot}} * \frac{T_{STP}}{Tr} \qquad 11$$

where V_r is the volume of the chamber, F_{tot} is the gas flow rate, T_{STP} is the standard temperature and T_r is the temperature of the chamber. As τ_{flush} is only dependent on the setups parameters, it does not account for the diffusion of oxygen inside the pores of the porous ceramics. The gas diffusion in porous ceramics has been extensively studied in the field of gas electrodes in fuel cells and electrolyzers[18,19]. This knowledge can be directly applied to an equilibration of pO_2 inside the pores of a ceramic material when performing relaxation experiments. To determine a time constant associated with gas diffusion in the pores, the diffusion coefficient of oxygen in the porous media must be defined. The Bosanquet equation[20] gives the efficient diffusion coefficient in a porous media as a function of the molecular diffusion coefficient $D_{O_2,N_2}^{\mathrm{Bulk}}$, and the Knudsen diffusion coefficient $D_{O_2,N_2}^{\mathrm{Knudsen}}$ of oxygen in porous media:

$$D_{O_2,N_2}^{eff} = \frac{p}{\chi} \cdot \left(\frac{1}{D_{O_2,N_2}^{Bulk}} + \frac{1}{D_{O_2,N_2}^{Knudsen}}\right)^{-1} \qquad 12$$

With p the porosity of the media, and χ the tortuosity factor of the gas phase. The molecular diffusion coefficient $D_{O_2,N_2}^{\mathrm{Bulk}}$ is defined with the empirical equation determined by Fuller and Gidding[21]:

$$D_{O_2,N_2}^{\mathrm{Bulk}} = \frac{10^{-3} \times T^{1.75}}{P\left(V_{O_2}^{1/3} + V_{N_2}^{1/3}\right)^2} \times \left(\frac{1}{M_{O_2}} + \frac{1}{M_{N_2}}\right)^{1/2} \qquad 13$$

With T the temperature, P the total pressure, V_x the molar volumes of the N_2 and O_2 molecules, and M_x their molar masses. The diffusion coefficient in the pores of a porous media $D_{O_2,N_2}^{\mathrm{Knudsen}}$ is defined by the Knudsen equation[22]:

$$D_{O_2,N_2}^{\text{Knudsen}} = \frac{1}{3} d_{\text{pore}} \left(\frac{8RT \times 10^7}{\pi M_{O_2}} \right)^{1/2} \quad 14$$

In which d_{pore} is the pore diameter. If the diffusion is considered to be in one dimension only (because the thickness of the ceramic is shorter than the length and width), a time constant associated to gas diffusion in the pores of the ceramic sample can be estimated with the following equation

$$\tau_{diff} = \frac{l^2}{4 \cdot D_{O_2,N_2}^{eff}} \quad 15$$

Where l is the sample thickness. Then, for any set of microstructural parameters (p, χ, d_{pore}, l) the time constant associated to gas diffusion in the porous sample can be calculated and compared with the flush time of the reactor. If τ_{diff} is lower than τ_{flush}, then the pO$_2$ inside the porous sample is at equilibrium with the rest of the gas phase in the reactor, and gas diffusion in the pores is not affecting the measurement. From equation 15, the pore diffusion time constant is calculated for a set of sample thickness and pore diameter values, and plotted in Figure 1a. Here, the tortuosity factor is set constant at x=1.5 consistent with tomography measurements on porous sintered ceramics for fuel cells[23]. Because the porosity should be open, we assume that it will always vary within narrow bounds, *i.e.* 20-40 %, for the technique to be successful. Therefore, the porosity is set constant to 30 %. Then, the time constant is calculated for sample thicknesses ranging from 100 µm to 1 cm, and for pore diameters ranging from 1 nm to 100 µm. For comparison, the typical time constant for flush time in our setup, calculated from equation 11, is represented as a line at 5 s. From this calculation, it is clear that the pore diffusion is never be limiting for the overall pO$_2$ equilibration, except for extreme cases of small pores and thick samples. Indeed, for the pore diffusion to become slower than the flush time, the sample should be at least 3 mm thick with pores in the range of 10 nm, or 1 cm thick for pores of 100nm, which is far from the typical experimental parameters targeted for the relaxation experiments. Assuming a fixed sample thickness of 1 mm (Figure 1b), such that it is typically prepared, the pore size should be in the range of 1 nm for pore diffusion to become limiting, which is not possible for sintered ceramics. Conversely, for a pore size of 1 µm (Figure 1c), which is typical for sintered porous ceramics, the sample thickness should be up to 2 cm for pore diffusion to become limiting, which is again far from realistic sample sizes.

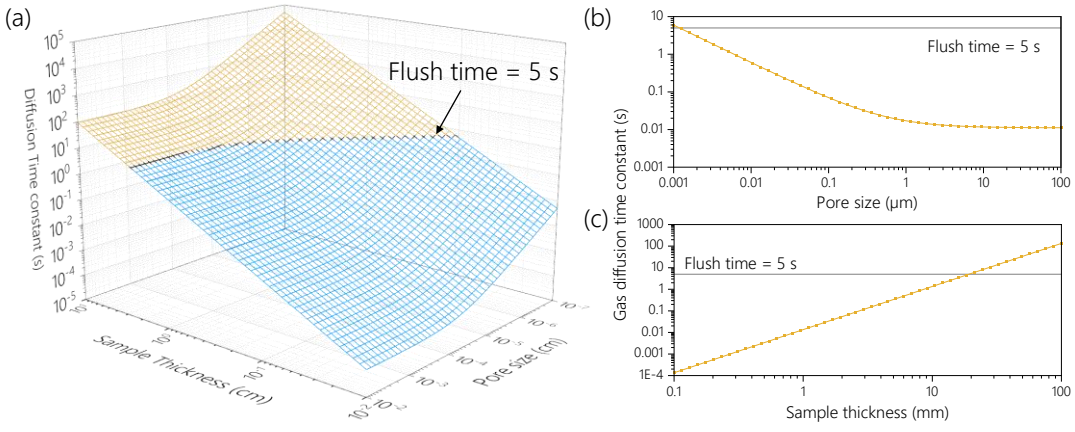

Figure 1: dependence of the time constant associated to gas diffusion with sample geometry. (a) 3D plot of τ_{gas} as a function of the sample thickness and the pore size. Individual dependence of τ_{gas} with (b) pore size at constant sample thickness of 1mm, and with (c) sample thickness at constant pore size of 1µm. The straight line corresponds to the time constant associated to the flush time.

Although pore diffusion is proven not to be limiting in realistic cases, the non-ideality of the step change of pO_2 due to the reactor flush time can still be taken into account in the relaxation model by a flush time correction proposed by Den Otter *et al.*[17]. The correction uses a convolution of equation 9 and 10 to yield the flush time corrected expression of the relaxation transient:

$$g(t) = 1 - \exp\left(\frac{t}{\tau_{flush}}\right) - \int_0^\infty f(R_n) \cdot \frac{\tau_n}{\tau_n - \tau_{flush}} \cdot \left[\exp\left(-\frac{2 \cdot k_{chem}}{R_n} \cdot t\right) - \exp\left(-\frac{t}{\tau_{flush}}\right)\right] \mathrm{d}R_n \qquad 16$$

Where $\tau_n = R_n / 2k_{kchem}$. This correction makes the technique more forgiving in terms of reactor design, because modifying the reactor design to decrease the flush time is not a simple task.

Although the model appears more complex than the initial one-time constant relaxation model, it does not add degrees of freedom in the fitting procedure. If the flush time is known and the radii distribution is defined *a priori*, the only fitting parameter is the surface exchange coefficient k_{chem}, which makes it less sensitive to the fitting procedure than fitting for D_{chem} and k_{chem} when measuring dense samples. Then, the model can be used in a simple least square fitting algorithm and does not require any optimization.

In the results section, both equation 9 and 16, *i.e.* the model without and with flush time correction, will be used for fitting the experimental data, and the relevance of the correction will be discussed. The model is fully implemented in a Matlab based application with a user-friendly interface, which does not require any computing skills and is available online[24]. Before being able to use this model on conductivity relaxation data, the actual grain size distribution of the samples to be measured has to be determined. The next section describes a simple protocol to determine the grain size distribution of porous ceramics, using simple electron microscopy images.

3 Results

3.1 Determination of the grain size distribution

Giving an accurate description of the microstructure is challenging, and may require heavy characterization tools such as FIB-SEM/3D image reconstruction, or X-ray tomography. Using such tools is contradictory to the purpose of this work to provide an easy-to-use protocol for reliable determination of oxygen surface exchange coefficients on mixed conducting oxide. Instead, in this section we describe a protocol to extract the relevant microstructural parameters of a porous ceramic from simple electron microscopy images to be later used in the conductivity relaxation model (equation 9 and 16).

The approach is to record images of a polished cross section of the porous ceramics and process them computationally using a method called “local thickness” initially proposed by Hildebrand and Rüesgsegger[25]. According to the authors, the local thickness at a given point in the structure is “the diameter of the largest sphere which includes the point and which can be fitted completely inside the structure”. Initially proposed for analyzing 3D images, the method can also be applied to polished cross section images. The advantage of this procedure is that it does not require a specific microstructure model, allowing it to be applied to any microstructure without prior assumption of a specific geometry (sphere, cylinders *etc.*).

This method, widely used in biology and medicine, is implemented in an open source software called Fiji, initially developed by Schindelin *et al.*[26] and is therefore accessible to anyone without prior knowledge in image processing computation. A detailed description of the computation of such procedure is available on the Fiji website[27]. Because the method requires binary images, it is necessary to record images with high contrast between the ceramic and the pores so that processing them into binary image is less user dependent. Thus, the samples are embedded in a resin and polished to a mirror

finish (details in the experimental section), and the images are recorded in back scattered electron mode to increase the contrast between the sample and the resin. The image processing follows three steps, all available in the Fiji software:

- A median filter to remove small artifacts
- A threshold to convert the image into a binary, black and white image
- The local thickness procedure, fully implemented in Fiji

The local thickness procedure returns a heat map of the microstructure in which the hotter colors correspond to the higher thicknesses and a histogram of the thickness distribution. In first approximation, the thicknesses returned by the technique can be defined as the diameter of the various cylinders, *e.g.* $R_n = L_t/2$ and can be used in equation 9 and 16. Then, the local thickness distribution can be fitted with an appropriate probability density function. In this work, all distributions can be accurately fitted with a lognormal distribution following eq 17:

$$f(L_t) = \frac{1}{\sigma\sqrt{2\pi}} \cdot exp\left(-\frac{1}{2} \frac{\left(ln\left(\frac{L_t}{\mu}\right)\right)^2}{\sigma^2} \right) \quad 17$$

In which μ is the median of the thickness distribution and σ is the shape parameter. This allows for an accurate definition of the microstructure from experimental SEM data, using only two parameters. Then, the lognormal distribution can be inserted in equation 9 and 16 to fully account for the microstructure of the porous ceramic. It is worth noting that the porosity and the specific area of the ceramics are not necessary to fit the conductivity transients anymore. For porosity, the model can be considered accurate when no closed pores are present (percolated porosity only). For specific surface area, it is a strong advantage to have an alternative, because specific surface area measurements such as nitrogen adsorption and Brunauer, Emmett, and Teller fittings are poorly reliable for low surface area samples, such as those considered in conductivity relaxation[28].

Figure 2 shows an example of the technique on a sample of Pr doped ceria, sintered at 1450 °C for 1 h and the corresponding unprocessed image (Figure 2a), after median filtering (Figure 2b), after applying the threshold (Figure 2c) and the heat map of the local thickness method (Figure 2d). Although this image analysis technique returns a thickness distribution that is accurately fitted with a lognormal distribution (Figure 2e), its fidelity to the "real" microstructure can be questioned if proper considerations are not taken during the procedure. Two main sources of inaccuracy can arise from this procedure: the threshold value with which the image is converted to a binary file, and the magnification of the original image. For the former, the sample preparation (polishing) and the contrast for recording the image is essential to reduce the uncertainty when choosing the right threshold value. Then, choosing the right threshold is usually done by gauging where the pore/ceramic limit is in term of grayscale value. Such an approach is user-dependent and may lead to errors. Instead, here we choose to define the threshold value that matches the actual porosity of the sample that can be readily determined from the mass and dimensions of the ceramic sample. Then, the threshold procedure is set from physical parameters and no longer depends on the user, thus limiting the risk of error. Because the threshold value is defined *a priori*, the procedure can be automated along with the local thickness procedure and repeated on more images. An ImageJ macro code to process images in batch is available in the supplementary information 2. This feature is a major benefit of the approach because it enables batch processing of a large number of images, in turn improving the statistical accuracy of the microstructure analysis.

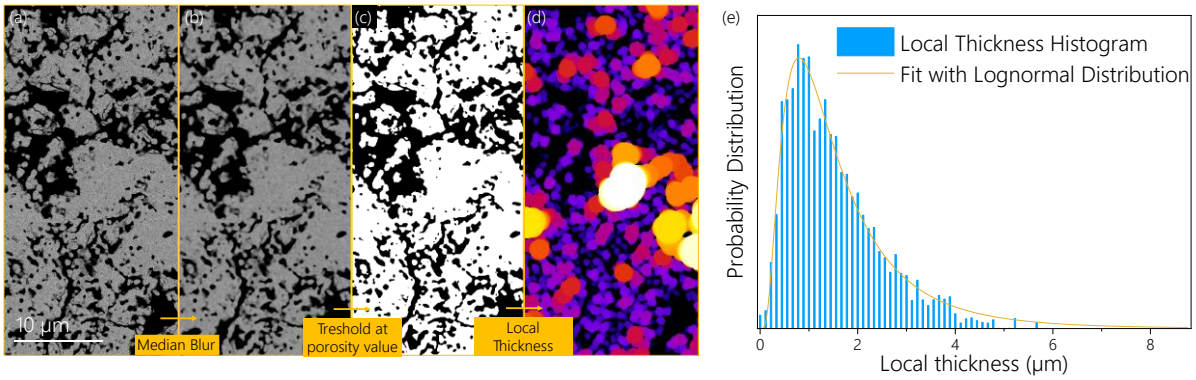

Figure 2: Example of the image processing technique used to return the local thickness distribution. (a) unprocessed image, (b) image after the median filter, (c) binary image after threshold, (d) heat map of the local thicknesses, (e) histogram of local thicknesses, fitted with a lognormal distribution.

However, the choice of magnification at which the images are recorded also requires careful considerations as it significantly influences the resulting thickness distribution. To determine the ideal magnification for the determination of thickness distribution, the image analysis procedure was performed on various magnifications ranging from ×500 to ×10,000, recorded on the same ceramic sample, and the results were compared. For each magnification 10 images with a resolution of 1024×768 pixels are used to study the scattering of thickness distribution. For each zoom, the thickness distributions determined on each image are also summed together and the sum of distributions is fitted with the lognormal distribution, to compare with the results of individual images. As an example of the output distribution from the local thickness procedure at various magnifications, Figure 3a and b show the images and summed thickness distributions of 10 images for three magnifications, namely ×500, ×3,000, and ×10,000. With low magnifications such as ×500, the thickness distribution returned by the procedure seems to be accurately fitted by the lognormal function, but the low resolution of the images tends to yield an overestimated grain size, because the median blur and threshold procedures erase the smaller features. Indeed, at this zoom the image resolution is only 4.5 $px \cdot \mu m^{-1}$, which means that for an average grain size in the range 1-3 µm, each grain is only a few pixels. For intermediate magnifications such as ×3,000, the fit with the lognormal function remains good, and the higher resolution of 27 $px \cdot \mu m^{-1}$ decreases the risk of overestimating grain sizes. For high magnifications such as ×10,000, the distribution is no longer fitted accurately with the lognormal distribution. Although the resolution is high (90 $px \cdot \mu m^{-1}$), the region of interest (image size) becomes too small to be a representative sample of the whole microstructure. As a result, the derived distribution varies dramatically from one image to another. Then, it appears mandatory to determine a parameters window for which the image analysis procedure yields trustworthy distributions. The two key parameters are the image resolution in $px \cdot \mu m^{-1}$, and the area of interest in μm^2. Then, such window should be made a function of the average grain size of the porous ceramic, since coarse and fine porous structures require different resolutions and areas of interest. This functional window can serve as a guideline for future users of this procedure.

To determine this functional window, the fitting results for all images and summed distributions for all magnifications were plotted as a function of the image resolution. Figure 3c shows the median thickness μ and the shape parameter σ derived from the distributions as a function of the resolution (and magnification). The figure represents the results for all individual images (hollow squares) as well as those of the summed distributions (filled squares) with their error bars. The median thickness appears to be strongly dependent on the resolution especially at lower magnifications. The median thickness evolution with the resolution can be fitted with a simple exponential decay function to show at which thickness the median converges. The dashed line represents the fit for individual images, while the solid line represents the fit of summed distributions. Such analysis shows that the median thickness converges to a value of 1.4 µm, and that considering individual images and summed distributions yields the same exponential fit. From such curve, we can propose a minimum resolution value for which the procedure is reliable, corresponding to the plateau of the exponential decay. For this sample, the resolution should

be at least 20 px·µm^{-1} in order for the procedure to be accurate. If this value is multiplied by the median thickness, one can define a more general rule for choosing the resolution depending on the sample microstructure: with the median thickness at 1.4 µm, the resolution should be at least 28 px per median grain size, for the procedure to be accurate.

The shape parameter of the distribution remains stable around $\sigma = 0.6$ regardless of the resolution, except for the highest magnification, *e.g.* ×10,000. At such magnification, the area of interest is too small compared to the average grain size, indicating that even for the summed distributions the area of interest is not representative of the whole microstructure. This is exemplified by the strong scattering of data points between single image distributions and by the dramatic decrease of goodness of fit (adjusted R^2), which drops to 0.4 for the summed distribution of the ×10,000 magnification. For a better assessment of the importance of the size of the area of interest to the reliability of the fitting procedure, the goodness of fit is plotted for single image distributions as well as for summed distributions, as a function of the area of interest, *i.e.* the image size in µm^2. For summed distributions, the considered area of interest is simply the sum of all image areas. For higher magnifications, some images were discarded because the threshold at a set value (the average porosity level) would fail for images were the porosity in the area of interest is actually higher or lower than the average porosity. Figure 3d shows the goodness of fit as a function of the area of interest for all magnifications. From such representation it is clear that the R^2 decreases dramatically below an area of interest of 1800 µm^2. Considering that the median diameters determined from the distributions converge toward a value of 1.4 µm, and assuming round grains, the cross section area of one grain should be in the range of 1.50 µm^2. From this estimate, we can propose that the area of interest should be at least one thousand times higher than that of the median grain cross section, for the procedure to yield reliable microstructural parameters.

To summarize, the image analysis should be done on images with a resolution of 28 pixels per median grain length and of a size of at least ×1000 times the area of an individual grain. With a fixed image resolution of 1024×768 pixels such criterion leaves a narrow window of magnification to perform this analysis, and summing the results of several images is mandatory to increase the area of interest. For subsequent samples, this criterion was used to select the most appropriate magnification and resolution to perform the image analysis. Alternatively, the SEM images can be recorded at a higher resolution, which allows considering lower magnification (high area of interest) without compromising on resolution. An example of a distribution of an image recorded at a magnification of ×500 and with a resolution of 12288×9216 pixels is given in the supplementary information (Figure S3-2). The distribution yields a median of $\mu = 1.38$ µm and a shape parameter of $\sigma = 0.68$, consistent with the results obtained on 1024×768 images. All images (Figure S3-1), distributions (Figure S3-2), and fit results (Table S3-1) used in this section are available in the Supplementary information.

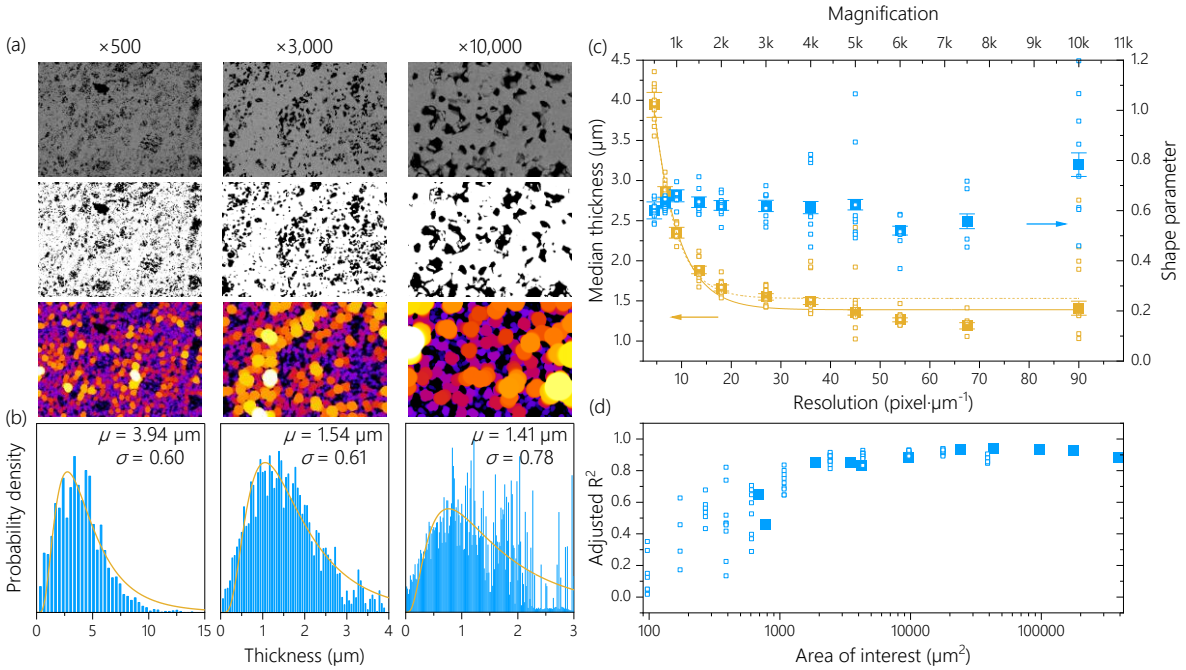

Figure 3 : Statistical analysis of the microstructure analysis with the local thickness procedure. (a) Primary image, binary image, and local thickness heat map for three representative magnifications: ×500, ×3,000, and ×10,000. (b) thickness distributions obtained after addition of 10 distributions for each magnification, and fit with the lognormal distribution. (c) Median thickness and shape parameter of the distributions as a function of the image resolution, for both individual (hollow squares) and summed (filled squares) distributions. (d) Adjusted R^2 (goodness of fit) of the fit with the lognormal distribution as a function of the area of interest. For summed distributions (filled squares) the area of interest is the sum of the area of all individual images for each magnification.

From this procedure, the microstructure of a porous mixed conducting oxide can be described with only two parameters, *i.e.* median thickness and shape parameter of the lognormal distribution, which are fixed in equation 9 and 16 for the model to fully account for microstructural features. As stated in the theory section (2.1), this model does not add any degree of freedom to the fitting procedure because the distribution is fixed, thereby improving its accuracy for the determination of k_{chem} than fitting with the distribution.

3.2 Simulation of relaxation transients

From these considerations, the model combining equations 16 and 17 can be used to simulate relaxation profiles and study the influence of various grain size distributions on the shape of the relaxation transients, for a fixed value of surface exchange coefficient k_{chem}. The profiles were simulated for a constant value of mean, median and mode grain radius, and systematic variation of the shape parameter of the distribution. The profiles are simulated for either a low value of k_{chem} (5×10^{-7} cm·s^{-1}) or a high value of k_{chem} (5×10^{-6} cm·s^{-1}). The time constant associated to flush time is set to 5 seconds, which is relevant to the measurement setup used in the experimental section.

In Figure 4 a, b and c, the simulation considers a constant mean value of grain radius, while modifying the shape parameter of the distribution. In this case the relaxation profiles are spreading on a narrow range, which suggests that the shape parameter does not influence the overall relaxation time of the return to equilibrium. However, the shape of the profiles is skewed significantly with higher shape parameter, indicating that the profiles would not be accurately described by a one-time constant model. Indeed, the profile corresponding to a shape parameter of 0 corresponds to such one-time constant model, and can be used as reference. It is also worth noting that for small shape parameters *i.e.* $\sigma = 0.1$, there is virtually no difference between the relaxation profile with and without the grain size distribution fit. Then, for samples with narrow grain size distribution a simple one-time constant model is sufficient to accurately describe the relaxation profiles.

In Figure 4 d, e and f, the simulation considers a constant mode value of grain radius, while modifying the shape parameter of the distribution. Contrary to constant mean simulations, the variation of shape parameter with constant mode yields a dramatic change of overall relaxation times for the simulated profiles. Again, because the profiles are skewed for high shape parameters, a fit with one time constant will not be satisfactory, except for small values such as $\sigma = 0.1$. The conclusions are the same for profiles simulated with a constant median grain radius (Figure 4 g, h, and i). From these simulations, it is clear that the model holds the potential to match a wide range of profile shapes, suggesting that it would be more suitable for fitting conductivity relaxation profiles measured on ceramics with heterogeneous microstructures. Additionally, profiles simulated with fast k_{chem} (Figure 4 c, f, and i) demonstrate the influence of adding the flush time correction in the model. Indeed, the flush time correction appears as a moderate inflexion in the early stage of the relaxation, demonstrating that the model can account for flush time artifacts when fitting profiles measured close to the flush time limit. The influence of the flush time is less obvious for slower k_{chem} (Figure 4 b, e, and h), suggesting that, in principle, the flush time correction would not be mandatory for fitting profiles measured far from the flush time limit.

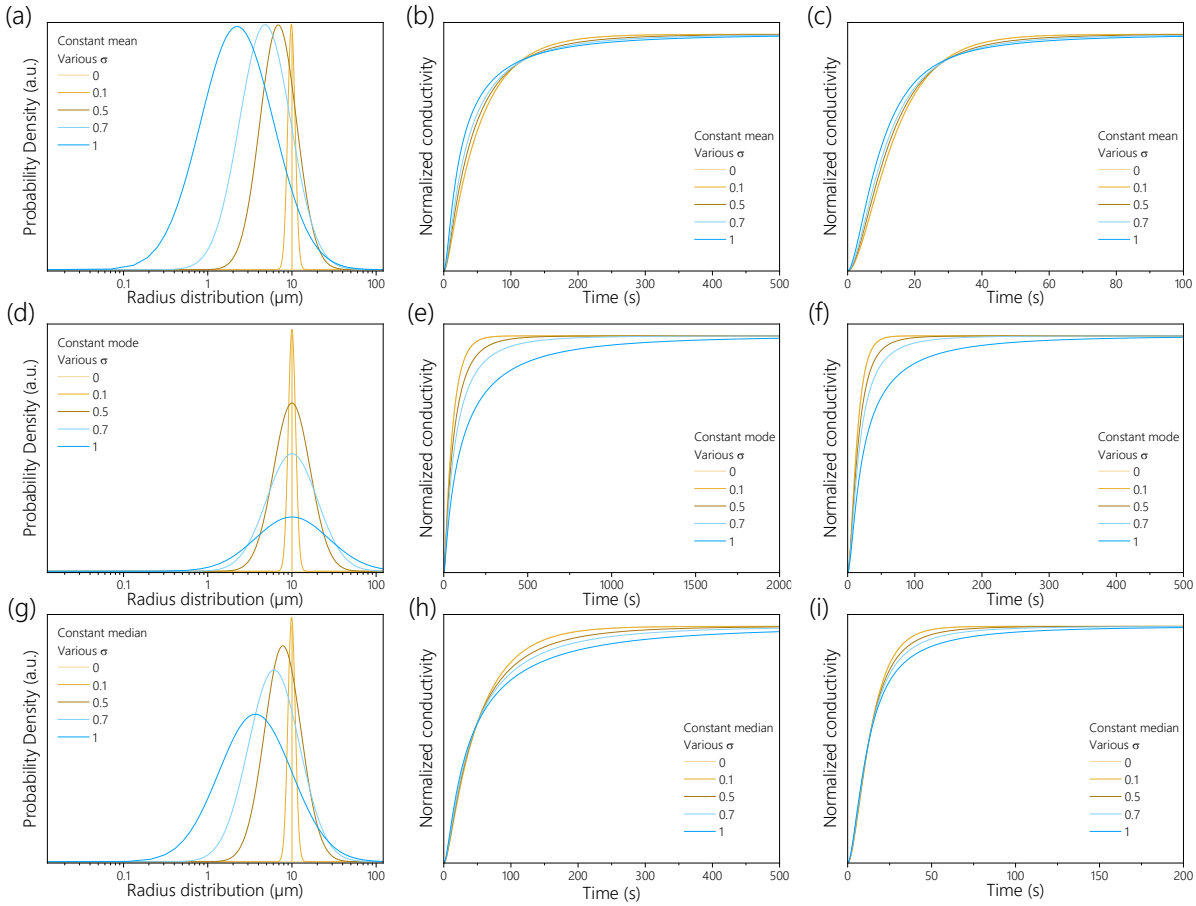

Figure 4: Simulated relaxation profiles for various grain size distributions. (a), (d), and (g) are the simulated distributions, (b), (e), and (h) are profiles generated with $k_{chem} = 5\times10^{-7}$ cm·s^{-1}, (c),(f), and (i) are profiles generated with $k_{chem} = 5\times10^{-6}$ cm·s^{-1}. All simulations consider a variation of shape parameter from 0 to 1. (a), (b), and (c) shows the simulation with a constant mean diameter, (d), (e), and (f) with a constant mode diameter, and (g), (h), and (i) with a constant median diameter.

Addressing the influence of flush time in these experiments is essential, as its influence on the reliability of the determination of kinetic coefficients in relaxation experiments has been thoroughly discussed in previous literature, by various authors[6–8,17]. More specifically, its influence was mainly discussed with respect to measurements of dense samples, where D_{chem} and k_{chem} can supposedly be determined simultaneously with a diffusion-based model. In this regard, Den Otter *et al.*[17] who first proposed the expression of the flush time correction, mentioned that : “to be neglected, the flush time should be at least 5000 times smaller than the duration of the relaxation experiment in the case of surface limited

regime". Such statement is strictly based on mathematical considerations, while using the analytical solution of the Fick second law of diffusion. In the case of porous samples, because the model is no longer based on a diffusion problem, the assessment of whether or not it is possible to neglect flush time has to be reconsidered. Here, we can make this assessment from simulating and comparing profiles with and without the flush time correction. Then, the profile generated with the flush time-corrected model can be back fitted without correction to measure the error that such omission produces. Repeating this protocol while decreasing k_{chem} allows defining maximum values where flush time can be neglected. Figure 5a presents an example of the procedure, where two profiles are generated with $k_{chem} = 10^{-6}$ cm·s^{-1} and $\tau_{flushtime} = 5$ s. One profile considers a monodisperse grain size of 10 µm, and the second a grain size distribution following the lognormal distribution with a median of 10 µm and a shape parameter of $\sigma = 1$. Both profiles are fitted without a flush time correction (equation 9). An error on k_{chem} (or its corresponding time constant) is calculated as

$$Error\ \% = \frac{k_{fit} - k_{sim}}{k_{sim}} \cdot 100 \qquad 18$$

In which k_{fit} is the oxygen surface exchange coefficient resulting from the fit without the flush time correction, and k_{sim} is the coefficient used to generate the profile with equation 16. Figure 5b shows the calculated error as a function of the simulated surface exchange coefficient. From such plot, one can define an error interval that is acceptable for their determination of k_{chem}. For example, we arbitrarily choose to consider that a 10 % error is reasonable in determining k_{chem}, which means that any profiles with time constants higher than $10\times\tau_{flush}$ (50 seconds in this case) can be fitted with equation 9 with good accuracy. In section 3.3, experimental data are fitted with both models to confirm the results of this simulation.

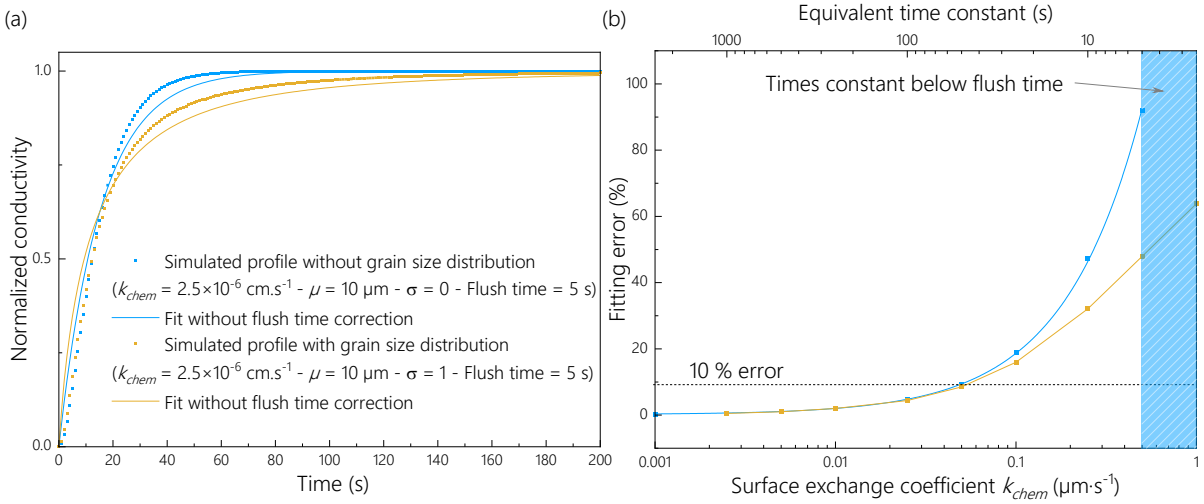

Figure 5: Influence of the flush time correction on fitting errors. (a) profiles simulated with a flush time with equation 16 are fitted without a flush time correction (equation 9) to evaluate the fitting error caused by neglecting the flush time. (b) Calculated error as a function of the oxygen surface exchange coefficient k_{chem} for an average grain size of 10 µm and a reactor flush time of 5 seconds.

3.3 Application to various mixed conducting oxides

From these considerations, both the image analysis procedure and the model can be applied to real ceramics samples. First, the accuracy of the model is studied in details on one Pr-doped ceria porous ceramic. Then, the broad applicability of the model to determine surface exchange kinetics coefficients is demonstrated on other mixed conducting oxides, *i.e.* $La_2NiO_{4+\delta}$ and $La_{0.6}Sr_{0.4}CoO_{3-\delta}$, and on a wide range of porous microstructure of Pr-doped ceria.

3.3.1 Detailed study of the fit results on Pr-doped ceria

A porous sample of $Pr_{0.1}Ce_{0.9}O_{2-\delta}$ was prepared by pressing and sintering a powder at 1450 °C for 1 h. The conductivity relaxation profiles were measured by 4-point conductivity in the temperature range

290 - 400 °C with pO_2 steps from 0.1 to 0.2 atm. A detailed description of the sample preparation and measurement is provided in the experimental section. The profiles were fitted with three models: a one-time constant model that does not account for grain size distribution but includes a flush time correction; the new model including grain size distribution but no flush time correction; and the full model including both the grain size distribution and the flush time correction. After recording and processing SEM images on the sample, the local thickness procedure described in section 3.1 returns a median thickness of μ = 1.4 µm and a shape parameter of σ = 0.68 that are fed into the model (detailed image analysis available in supplementary information SI3). Additionally, the standard errors obtained when determining the median and shape parameter are used to calculate high and low boundaries of these parameters, that are then propagated into the fit of kchem to assess the error on kchem from the grain size distribution. Such procedure shows that the error from the grain size distribution is roughly 4 %. For all other samples presented in the next sections, such error was always below 8 %, which is small enough to not affect error bars significantly.

Figure 6 shows the relaxation profiles measured at low (b), mid (c), and high (d) temperature (324 °C, 345 °C, and 397 °C, respectively), along with the fits with the three models. At those example temperatures, the full model undoubtedly fits the data better than the model without the grain size distribution, illustrated by the plot residual remaining below 1 % at any stage of the transient and for all temperatures. As both models only fit for k_{chem}, such result is remarkable because it suggests that both the microstructure analysis *via* the local thickness procedure and the relaxation model are capable of giving an accurate representation of oxygen exchange in porous ceramics, which were often believed to be too complicated to be described with simple models. Additionally, the comparison between the models with (full model) and without flush time correction shows that the influence of flush time is higher at high temperature, when the time constants associated to the oxygen exchange reaction approach that of the flush time. This is in agreement with the observations made in the simulation section (3.2). On the residual plot it can be noted that for the intermediate temperature (345 °C) the error is high at the early stage of the transient. This is consistent with observations from measurements on dense ceramics[17]. However, the confidence interval of $10 \times \tau_{flush}$ discussed in the simulation section is not necessary when the flush time correction is integrated to the model. Indeed, at 397 °C the time constant associated to the reaction is around 10 s, which is only $2 \times \tau_{flush}$, yet the fit residual is under 1 % with the flush time correction, indicating that the model can accurately account for both the flush time and the reaction time constants even for fast transients.

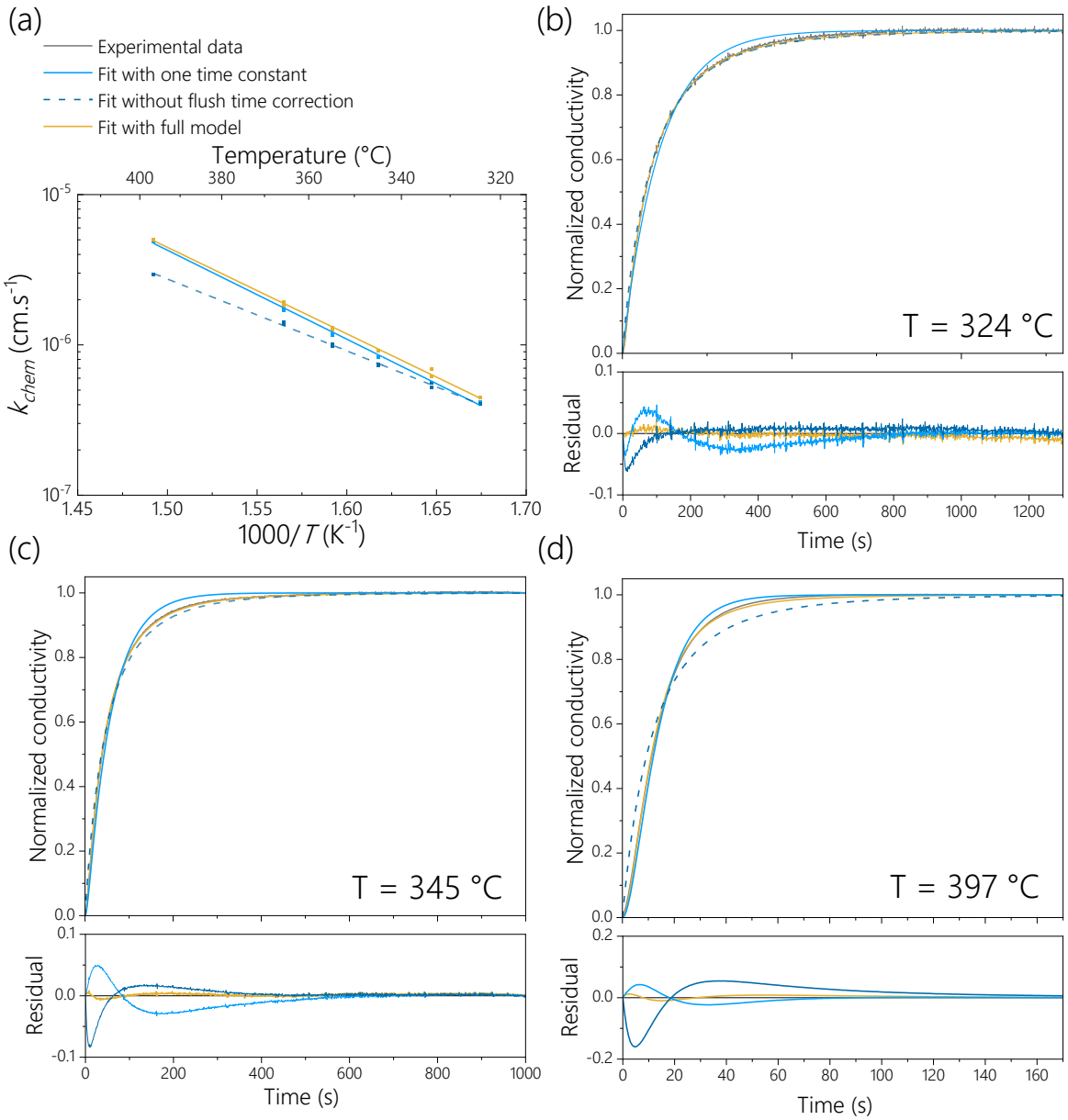

Figure 6: Application of the model to a Pr-doped ceria porous ceramic. (a)Temperature dependence of k_{chem} as a function of the fitting procedure, examples of relaxation profiles and the corresponding fits with the three models for transients measured at (b) 324 °C, (c) 345 °C, and (d) 397 °C.

The values of oxygen surface exchange k_{chem} derived from each fitting procedure can also be compared. Figure 6a shows the k_{chem} values as a function of temperature, calculated from the three models considered: no distribution but flush time correction, distribution but no flush time correction, and the full model with both distribution and flush time correction. Surprisingly, the classical model that does not account for the grain size distribution yields similar k_{chem} values than that of the full model, but with slightly overestimated values. As mentioned in the simulation section, this feature probably holds for relatively narrow grain size distribution, but the difference between both models should be significant for broader grain size distributions. Moreover, even if the simple model yields similar k_{chem} than the full model, the fact that the fits are less accurate leaves doubts regarding whether the derived k_{chem} are truly representative of the materials properties. With the full model, such doubt is eliminated, increasing the trustworthiness of the technique for measuring k_{chem} values. The comparison between k_{chem} values derived from the full model and from the model without flush time correction shows a substantial difference, both in terms of values, and more importantly in terms of activation energy. Indeed, as the flush time is temperature independent, its weight in the overall time constant of the transient increases

with temperature. In turn, the error made without accounting for flush time increases with temperature, and the derived k_{chem} shows a dramatic change of activation energy, which is in fact just a measurement artifact. Activation energies of reaction coefficients are the cornerstone of mechanistic interpretation of catalytic properties of materials. Ultimately, such artifacts lead to misinterpretations of catalytic properties of materials. As the full model properly accounts for such artifacts, the derived activation energy of k_{chem} is more trustworthy.

3.3.2 Application to other mixed conducting oxides

Although the model accurately fits the transients recorded on one $Pr_{0.1}Ce_{0.9}O_{2-\delta}$ sample, such result is not sufficient to demonstrate the broad applicability of the method to other materials and microstructures. Therefore, two other mixed conducting oxides were considered for this procedure, namely $La_2NiO_{4+\delta}$ and $La_{0.6}Sr_{0.4}CoO_{3-\delta}$. Then, the results obtained with the full model were compared with literature data, derived from conductivity relaxation on dense samples. Because $La_{0.6}Sr_{0.4}CoO_{3-\delta}$ show fast oxygen exchange kinetics, it is preferable to prepare a porous ceramic with coarser grain, so that measurable transients can be obtained at intermediate temperatures. For this material, a starch pore former is added to the pellet before sintering, which enables the preparation of ceramics with grain/pores in the range of 10-100 µm. The preparation of the porous ceramic samples is detailed in the experimental section. Fitting results at all temperatures are available in the supplementary information (SI5). Figure 7 shows the results for $La_2NiO_{4+\delta}$ (a, b and c) and $La_{0.6}Sr_{0.4}CoO_{3-\delta}$ (d, e, f). The summed thickness distribution obtained after adding the local thickness distributions of 3 images. For $La_2NiO_{4+\delta}$ the images were recorded at a magnification of ×2500, yielding a resolution of 10 pixels per grains and an area of interest of ×1000 the grain surface. For $La_{0.6}Sr_{0.4}CoO_{3-\delta}$, the images were recorded at a magnification ×100, resulting in a resolution of 30 pixels per grain and an area of interest ×3000 larger than the grain surface. For both samples the image analysis is done within the bounds determined in section 3.1. The distributions (Figure 7a) and d) can be accurately fitted with a lognormal distribution function, with a R^2 of 0.92 for $La_2NiO_{4+\delta}$ and R^2 = 0.85 for $La_{0.6}Sr_{0.4}CoO_{3-\delta}$. The median and shape parameter for $La_2NiO_{4+\delta}$ are μ = 0.32 µm and σ = 0.46, and μ = 34.6 µm and σ = 0.64 for $La_{0.6}Sr_{0.4}CoO_{3-\delta}$. Following the same procedure used in the case of $Pr_{0.1}Ce_{0.9}O_{2-\delta}$, the median and the shape parameter are fed into the full relaxation model (equation 16) to fit the relaxation transient. Examples of typical transients are shown in Figure 7b and e to illustrate that the model accurately fits the transients for both materials. Considering that the microstructure of $La_2NiO_{4+\delta}$ and $La_{0.6}Sr_{0.4}CoO_{3-\delta}$ are markedly different from that of $Pr_{0.1}Ce_{0.9}O_{2-\delta}$, and from each other, with median grain size varying from 1.5 µm to 0.32 µm in the case of $La_2NiO_{4+\delta}$ and 34.6 µm in the case of $La_{0.6}Sr_{0.4}CoO_{3-\delta}$, the applicability of the model to such a range of materials and microstructures is remarkable. Then, the k_{chem} values obtained from the model are plotted as a function of temperature and compared with literature data. In Figure 7c, the oxygen surface exchange coefficients k_{chem} of $La_2NiO_{4+\delta}$ measured on porous ceramics are slightly lower than those measured on dense $La_2NiO_{4+\delta}$ samples[29], while the activation energy is the same (E_a = 1.43 ± 0.01 eV). In the case of $La_{0.6}Sr_{0.4}CoO_{3-\delta}$ (Figure 7f), k_{chem} values measured on porous ceramics and with this model are significantly higher than those obtained on dense ceramics by Tripković *et al.*[30] and the activation energy is slightly higher (E_a = 1.41 ± 0.03eV in this study and E_a = 1.26 ± 0.07 eV for Tripković *et al.*[30]). The errors associated with the activation energies are the standard error of the linear fit of the Arrhenius plot of k_{chem}. Discrepancies with data obtained on dense samples should not be analyzed as inaccuracy from the proposed technique, as such discrepancies were already observed between literature data on only dense samples[30,31]. Rather, the reactivity of the surface of porous ceramics could be dramatically different from a polished surface. This calls into question whether polished dense samples can truly be considered to have a "pristine" surface that can characterize oxygen surface exchange kinetics of a mixed conducting oxide. First, a polished surface can be considered as a cleaved surface, with terminations that are out of equilibrium, whereas a porous ceramic has a fully relaxed surface because it was prepared at high temperature. Second, polishing with diamond and alumina suspensions can leave impurities occlusions on the surface that can modify the reactivity

toward the oxygen exchange reaction. This could explain why k_{chem} measured done on porous $La_2NiO_{4+\delta}$ and $La_{0.6}Sr_{0.4}CoO_{3-\delta}$ are higher than the dense references. Finally, porous structures are more representative of the material as it would be used in an application such as a fuel cell electrode, a sensor, *etc*. Thus, it is mandatory to repeat the measurements and fitting procedures on a variety of microstructures to study the potential scattering of k_{chem} values with surface morphology features, that is, after correcting for the grain size distribution.

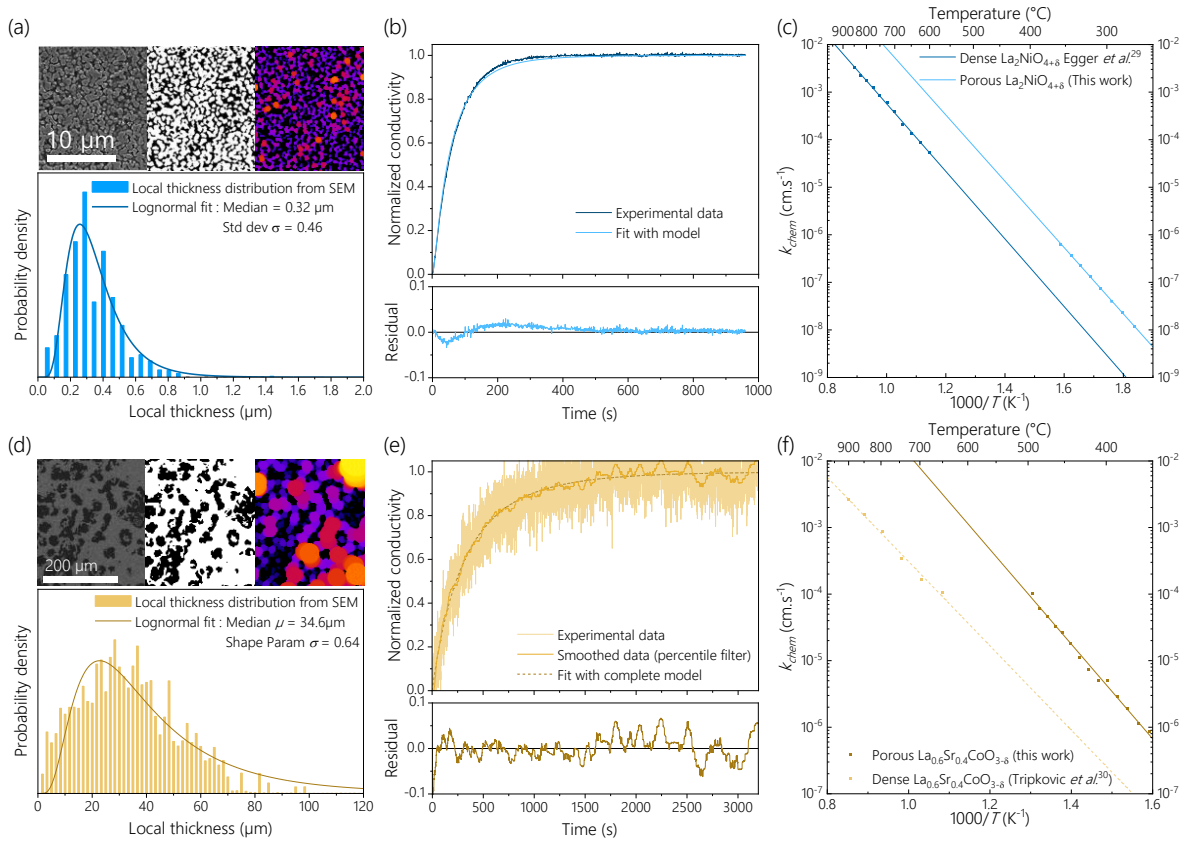

Figure 7 : Application of the procedure to $La_2NiO_{4+\delta}$ and $La_{0.6}Sr_{0.4}CoO_{3-\delta}$. For $La_2NiO_{4+\delta}$:(a) Polished cross section image, binary image and local thickness heat map and derived thickness distribution (b) typical relaxation transient fitted with the model and with a simple one time constant exponential for comparison. (c) k_{chem} as a function of temperature for $La_2NiO_{4+\delta}$ compared with data from the literature[29]. (d) (e) and (f) are the same figure than (a) (b) and (c) but for $La_{0.6}Sr_{0.4}CoO_{3-\delta}$. As the noise level is high for $La_{0.6}Sr_{0.4}CoO_{3-\delta}$, a percentile filter was applied to smooth the experimental data.

3.3.3 Application to various microstructures

To demonstrate the broader applicability of the model and to study the potential effect of surface morphology features mentioned in the previous section, a wide range of microstructures were prepared from a $Pr_{0.1}Ce_{0.9}O_{2-\delta}$ powder, measured by conductivity relaxation, and the transient were fitted with the model. Three preparation protocols were considered: *i)* pressing and single step sintering at 1200 °C, 1300 °C, 1350 °C, and 1450 °C for one hour; *ii)* a grain coarsening treatment of the powder (at the same temperatures), followed by grinding, pressing, and a second sintering step at 1450 °C for one hour; *iii)* addition of a cellulose pore former to the powder, followed by a debinding step at 1000 °C for 1h in O_2 and a final sintering at 1450 °C for one hour. Figure 8a shows the polished cross sections of 8 Pr doped ceria samples produced from these three protocols. Details of the fitting procedure for determining grain size distributions for each sample is available in the supplementary information (SI4). Figure 8b shows the lognormal distributions of each samples, derived from fitting the local thickness distributions, which demonstrate that the three protocols yielded microstructures with mean grain size ranging from 200 nm to 50 µm. Additionally, all samples remain sufficiently porous for the relaxation measurements to be valid, *i.e.* with porosity ranging between 20 and 40 %. After conductivity relaxation measurements are completed on all samples, the oxygen surface exchange coefficient is derived from fitting the transient

with the complete model (equation 16), and using median grain size and shape parameters from the log normal distributions (all transients and fits for all samples and temperatures are available in the supplementary information SI5). Figure 8c shows the temperature dependence of the oxygen surface exchange coefficients k_{chem}, for all the prepared porous ceramics, along with our previous reference[11] and that of Schaube *et al.*[32]. The most remarkable observation is that regardless of the grain size distribution, the derived k_{chem} values for all samples fall on two distinct lines, both of which show distinct activation energies. The first population of k_{chem} values corresponds to samples prepared with two steps sintering, and results in lower k_{chem} values but lower activation energies. For those samples, it seems that the model accurately accounts for the grain size distribution as the derived k_{chem} are identical (within experimental error), and their activation energy is E_a = 1.0 ± 0.1 eV. The second population of k_{chem} values corresponds to the samples prepared using only one sintering step. Again, the k_{chem} values appear to be independent of the grain size distribution of the porous ceramics, validating the applicability of the model on a wide range of porous ceramics. This population of sample shows a higher activation energy for k_{chem}, *e.g.* E_a =1.4 ± 0.1 eV, that is significantly higher than for samples prepared with two sintering steps. The last sample, prepared with a pore former and showing a mean grain size of 30 µm, yields k_{chem} values of the same order of magnitude as that of the samples prepared with one sintering step. Such result is remarkable, considering that the difference of mean grain size between the two types of samples can reach up to three orders of magnitude. Again, it emphasizes the robustness of the model and procedure in determining oxygen surface exchange coefficients that are essentially independent of the grain size distribution.

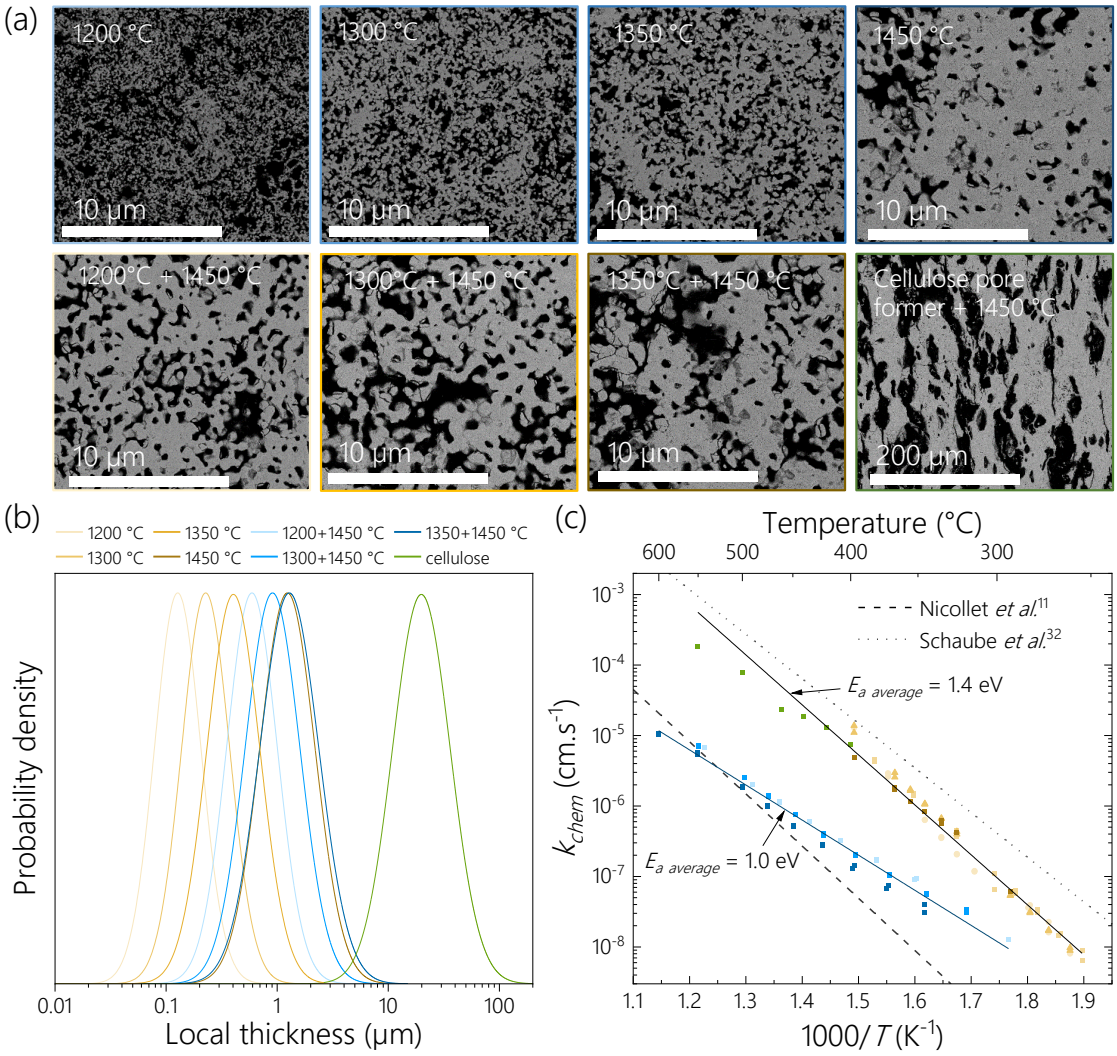

Figure 8 : Application of the procedure to various microstructure of porous Pr-doped ceria ceramics. (a) SEM images of the polished cross sections for all samples. (b) Lognormal distributions of all samples derived from fitting the local thickness distributions. (c) Oxygen surface exchange coefficient k_{chem} as a function temperature for all samples, compared with data from the literature[11,32].

Although such result is promising, it is necessary to discuss possible reasons to explain the two different populations of k_{chem} derived with this method. As the two populations correspond to samples prepared by two distinct methods, we focus the discussion on the differences that those two methods can produce in term of microstructure regardless of simple size distributions. Indeed, further observation by electron microscopy of fractured cross section (Figure 9) shows substantial differences in grain shape that correspond strikingly to the two populations of k_{chem} values and the two preparation methods. For samples prepared with one step sintering, the ceramics are made of faceted grain resembling pyramidal shapes. Such grains have been studied for pure ceria and correspond to a crystal growth in the (111) orientation[33]. For samples prepared by two step sintering, the grains are round, showing no particular grain orientation or faceted crystals. Such difference can arise from the intermediate grinding step that is necessary in the two step sintering procedure. Such a grinding step can erode the corners and edges of faceted grain and erase the preferential crystal orientation, which is further suppressed by the second sintering step. For the sample prepared with pore former, it is also prepared following a single sintering steps, and its k_{chem} values fall on the population of k_{chem} of samples prepared with a single step sintering. Although this sample does not show faceted grains, its large grains are primarily terminated with steps and terraces, which also point to a preferential crystal orientation.

A second hypothesis can explain the lower k_{chem} values for samples prepared with the two step sintering procedure. The additional grinding step is performed in an agate mortar, which could introduce SiO_2 pollutions into the sample. Such pollution is known to decrease the surface exchange coefficient[11,34]. Although those two hypotheses are not definitive, they emphasize the fact that oxygen surface exchange coefficients cannot be considered as intrinsic transport characteristics of a material, such as it is often assumed. It is in fact heavily dependent on surface chemistry, and our technique provides a valuable tool to study the link between surface chemistry and oxygen reaction kinetics. From the assumption that k_{chem} is extrinsic by nature, this study comes in conflict with measurements done on polished dense samples. Indeed, such studies assume that a polished surface is sufficient prevent microstructure effects (*i.e.* mostly roughness and grain size) and access a "pristine" value of such coefficient. In fact, we suggest that polished dense surfaces are yet another microstructure, which cannot necessarily represent the behavior of the material toward surface oxygen exchange. Such surfaces are actually cleaved, and most likely out of equilibrium, and therefore not an ideal case study for measurement of reaction kinetics; this point has already been discussed previously in the case of $La_{0.6}Sr_{0.4}CoO_{3-\delta}$[30].

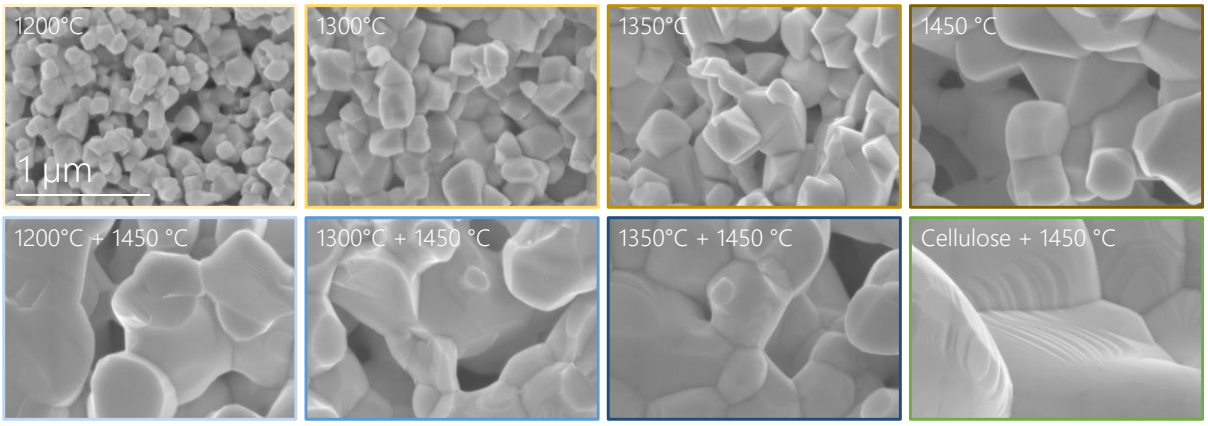

Figure 9: SEM images of fractured cross sections of Pr-doped ceria porous ceramics with various microstructures.

4 Conclusion

Oxygen surface exchange coefficients on mixed conducting oxides are challenging to determine in a reliable way. In this work we proposed a new procedure which is both accessible and inexpensive, to determine such coefficient on porous samples. The procedure involves simple 4-point conductivity measurements to record conductivity relaxation transients after a step change of oxygen pressure. With a simple image analysis procedure called local thickness applied to images recorded by scanning electron microscopy, the sample microstructure can be described by a grain size distribution. Then, a new analytical model that accounts for both microstructure and gas diffusion is proposed. Such model can be applied to a wide variety of materials and microstructure, yielding k_{chem} values that are essentially independent of the grain size of the porous ceramic. Given that the grain size of porous ceramics can be accounted for accurately, this technique opens new opportunities to study other surface chemistry features that can affect the rates of oxygen exchange on mixed conducting oxides, namely the grain shape and potential surface pollution that are ubiquitous in ceramic materials. In the case of unknown materials, we suggest that studies of k_{chem} with the presented method is run in parallel with studies of the diffusion coefficient on dense sample (also by conductivity relaxation). This will allow calculating an estimate of the characteristic length and assess the validity of the measurement *a posteriori*. The image analysis procedure is readily available for anyone without prior knowledge of computational image analysis, and the fitting procedure of the relaxation transient is fully implemented in a user-friendly application featuring a graphical user interface that does not require knowledge of computing techniques. This application is available here: https://github.com/Clement-Nicollet/GLORIA-app.git.

5 Acknowledgment

The authors acknowledge the French national research agency for their financial support through the project ANR-21-CE50-0020. The authors thank Ashley Nicollet for helping in reviewing the manuscript.

6 Author contributions

C.N. developed the original idea, designed the experimental protocol, prepared the samples, built the experimental set-up, performed the conductivity relaxation and SEM measurements, wrote the code for data processing, wrote the first draft and supervised the work. C.M. proposed the image analysis protocol and helped with the interpretation of the results. S.G., A.M., and I.A. contributed to the preparation of porous ceramic samples and conductivity measurements. All co-authors reviewed the manuscript.

7 Experimental

7.1 Sample preparation

The $Pr_{0.1}Ce_{0.9}O_{2-\delta}$ powder was prepared by a citrate-nitrate combustion synthesis. $Pr(NO_3)_3$; 6 H_2O (99.9 % Aldrich) and $Ce(NO_3)_3$; 6 H_2O (99.5% Reacton) are dissolved in deionized water. Citric acid was added to the solution in a ratio 0.3 with nitrate ions. The solution was evaporated at 120 °C overnight on a hot plate, and heated to 300 °C to trigger the combustion reaction. The resulting ashes were crushed in an agate mortar and calcined at 600 °C for 3 h. Then, the powder was ground in an agate mortar and acetone for one hour to break the foam-like agglomerates formed during the combustion.

The same procedure was used for preparing $La_{0.6}Sr_{0.4}CoO_{3-\delta}$ powders, but with different fuel and fuel/nitrate ratio. $La_{0.6}Sr_{0.4}CoO_{3-\delta}$ was prepared with glycine as fuel in a G/N ratio of 1.2. The final powder was annealed at 1000 °C for 3 hours in air to crystallize the single phase perovskite. For $La_2NiO_{4+\delta}$, a commercial power from Marion Technologies was used.

The porous ceramics for conductivity relaxation were prepared following three protocols: single sintering, two step sintering, and pore-forming sintering. In the single sintering procedure, the powder was pressed in a 20 mm diameter die at a uniaxial pressure of 1 t, and sintered in air at various sintering temperatures for one hour. In the two-step sintering procedure, the first step was identical to the single sintering procedure. Then, the sintered pellet was ground in an agate mortar for 30 min, pressed again

into a pellet (20 mm diameter) at a pressure of 5 t (a coarse powder requires a higher pressure to form a pellet) and with addition of water (50 µL per gram of powder) to improve the mechanical stability of the green pellet. The second sintering step was done in air at various temperature, for one hour. For LNO, the commercial powder was pressed into a 20mm at 1 t of uniaxial pressure and sintered at 1200 °C for 6 h. The pore-forming sintering procedure used cellulose (SigmaCell 50 µm, Aldrich) for $Pr_{0.1}Ce_{0.9}O_{2-\delta}$ and starch (Prolabo) for $La_{0.6}Sr_{0.4}CoO_{3-\delta}$ as pore formers. The pore former was added to the ceramic powder in the ratio 50 vol.% for $Pr_{0.1}Ce_{0.9}O_{2-\delta}$ and $La_{0.6}Sr_{0.4}CoO_{3-\delta}$. The powder and pore-former were dry mixed in an agate mortar for 15 min. Then, the ceramic/cellulose mixture was pressed (20 mm die) at 1 t to form a green pellet. The pellet underwent a debinding treatment at 1000 °C for 1 h in O_2 to burn the pore former (with heating and cooling ramps of 1 °C.min^{-1}). Then, the pellets were sintered at high temperature: 1450 °C for 6 h for $Pr_{0.1}Ce_{0.9}O_{2-\delta}$, 1300 °C for 10 h for $La_{0.6}Sr_{0.4}CoO_{3-\delta}$. The pellets were cuts into bars with a diamond low speed disc saw. The dimensions of the bars were roughly 20×3×1 mm for all materials. For conductivity measurements, four gold wires were wrapped around the bar sample 5 mm apart. A gold paste was applied on the wires to improve current collections, and the samples were mounted into the conductivity measurement setup to be annealed in-situ at 600 °C for 2 hours.

7.2 Conductivity relaxation measurements

The conductivity relaxation measurements were performed in a home-made conductivity setup. An outer alumina tube (diameter 25 mm - length 60 cm) was set into a tube furnace (homemade), and sealed with KF25 flanges. A sample holder with four Pt wires and a S thermocouple was fitted into the tube through another KF25 flange. The temperature was controlled with an Eurotherm 3216 PID controller. The gas composition was controlled by mixing high purity O_2 and N_2 (Alfagaz 2 – Air liquide) with two mass flow controllers (Brooks GF40) at a total flow rate of 300 sccm. The pO_2 step were controlled directly on the gas flow controllers by changing the set points simultaneously. All pO_2 step in the study were from 0.1 to 0.2 atm. The electrical resistance of the sample was measured with a Keithley 2450 source meter, set in constant voltage at 0.5V for $Pr_{0.1}Ce_{0.9}O_{2-\delta}$, and constant current of 0.05 A for $La_2NiO_{4+\delta}$ and 1 A for $La_{0.6}Sr_{0.4}CoO_{3-\delta}$. In the case of $La_{0.6}Sr_{0.4}CoO_{3-\delta}$, a seemingly high current of 1 A results in Voltage drops below 10mV, which is low enough to avoid Joule heating of the sample. The temperature, gas flows, and electrical measurements were controlled with a custom program that enabled automatic measurements.

An important parameter to consider for the technique to be reliable is to avoid poorly sintered ceramics, because narrow sintering necks between grains can lead to current constrictions effects that will make the equivalence between electrical resistance and oxygen vacancy concentration more questionable. To ensure that current constriction is not an issue, the conductance of the sample can be corrected for porosity, and compared to the conductivity of a dense sample. If they are comparable, current constriction is not an issue and the relaxation experiments are reliable.

The measurements were performed after annealing the gold contact at 600 °C, while decreasing the temperature. For each temperature step, the sample is left to stabilize for 2 hours before the pO_2 steps. Then, two cycles of pO_2 steps (0.1 → 0.2 → 0.1 atm) were performed to record two relaxation transients for each temperature. To assess the time constant of the pO_2 step, *i.e.* the flush time, the samples were measured at high temperature where their oxygen exchange kinetics are not limiting, which means that the resistance transient is only limited by the flush time. This measurement yielded a time constant associated to flush time of τ_f = 5 s, and was consistent throughout all measured samples. Such consistency also confirmed that the gas diffusion in the pores of the samples was not limiting the exchange kinetics, and that pO_2 in the pores is at equilibrium with the rest of the reactor volume.

7.3 Electron microscopy

For microstructure analysis, the samples were measured by scanning electron microscopy. First, the samples were fractured, cleaned in ethanol in a sonication bath, and embedded in an epoxy resin (Epofix,

Struers). After pouring the resin on the sample placed into a mold, the latter was set under primary vacuum for 40 min to remove trapped bubbles. Several vacuum/vent cycles were performed to improve the penetration of the resin into the pores of the samples. Then, the resin was left to set overnight in ambient air. After drying, the resin was sanded with SiC abrasive paper with decreasing grit size (800, 1200, and 4000), and polished with felt disc (MD-Mol Struers) and diamond suspensions of 9 µm, 6 µm, 3 µm and 1 µm for 10 minutes each. The resin was cleaned in a sonication bath for 5 min between each suspension.

The images were recorded on a Zeiss Merlin scanning electron microscope, at an acceleration voltage of 5 kV and a working distance of 6 mm. All polished cross sections images were recorded in back scattered electron mode to enhance the contrast between the pores and the ceramic, which improve the reliability of the subsequent image analysis. The fractured cross sections images were recorded in secondary electron mode.

8 References

1. Adler, S. B. Factors governing oxygen reduction in solid oxide fuel cell cathodes. *Chem. Rev.* **104**, 4791–4843 (2004).
2. Chueh, W. C. *et al.* High-flux solar-driven thermochemical dissociation of CO_2 and H_2O using nonstoichiometric ceria. *Science* **330**, 1797–1801 (2010).
3. Bouwmeester, H. J. M., Kruidhof, H. & Burggraaf, A. J. Importance of the surface exchange kinetics as rate limiting step in oxygen permeation through mixed-conducting oxides. *Solid State Ionics* **72**, 185–194 (1994).
4. Wang, C., Yin, L., Zhang, L., Xiang, D. & Gao, R. Metal oxide gas sensors: Sensitivity and influencing factors. *Sensors* **10**, 2088–2106 (2010).
5. Staerz, A., Weimar, U. & Barsan, N. Current state of knowledge on the metal oxide based gas sensing mechanism. *Sensors and Actuators B: Chemical* **358**, 131531 (2022).
6. Ten Elshof, J. E., Lankhorst, M. H. R. & Bouwmeester, H. J. M. Oxygen Exchange and Diffusion Coefficients of Strontium-Doped Lanthanum Ferrites by Electrical Conductivity Relaxation. *J. Electrochem. Soc.* **144**, 1060–1067 (1997).
7. Ciucci, F. Electrical conductivity relaxation measurements: Statistical investigations using sensitivity analysis, optimal experimental design and ECRTOOLS. *Solid State Ionics* **239**, 28–40 (2013).
8. Cox-Galhotra, R. A. & McIntosh, S. Unreliability of simultaneously determining kchem and Dchem via conductivity relaxation for surface-modified $La_{0.6}Sr_{0.4}Co_{0.2}Fe_{0.8}O_{3-\delta}$. *Solid State Ionics* **181**, 1429–1436 (2010).
9. Li, Y., Gerdes, K., Diamond, H. & Liu, X. An improved method to increase the predictive accuracy of the ECR technique. *Solid State Ionics* **204–205**, 104–110 (2011).
10. Ganeshananthan, R. & Virkar, A. V. Measurement of surface exchange coefficient on porous $La_{0.6}Sr_{0.4}CoO_{3-\delta}$ samples by conductivity relaxation. *J. Electrochem. Soc.* **152**, A1620–A1628 (2005).
11. Nicollet, C. *et al.* Acidity of surface-infiltrated binary oxides as a sensitive descriptor of oxygen exchange kinetics in mixed conducting oxides. *Nat Catal* **3**, 913–920 (2020).
12. Zhang, Y., Yan, F., Hu, B., Xia, C. & Yan, M. Chemical relaxation in porous ionic–electronic conducting materials represented by the distribution of characteristic times. *J. Mater. Chem. A* **8**, 17442–17448 (2020).
13. Han, H. *et al.* Method to determine the oxygen reduction reaction kinetics *via* porous dual-phase composites based on electrical conductivity relaxation. *J. Mater. Chem. A* **11**, 2460–2471 (2023).
14. Han, H., Jiang, Y., Zhang, S. & Xia, C. Perspective on high-temperature surface oxygen exchange in a porous mixed ionic-electronic conductor for solid oxide cells. *Phys. Chem. Chem. Phys.* **25**, 12629–12640 (2023).
15. Maier, J. Interaction of oxygen with oxides: How to interpret measured effective rate constants? *Solid State Ionics* **135**, 575–588 (2000).
16. Lu, Y., Kreller, C. & Adler, S. B. Measurement and modeling of the impedance characteristics of porous $La_{1-x}Sr_xCoO_{3-\delta}$ electrodes. *J. Electrochem. Soc.* **156**, B513–B525 (2009).

17. Den Otter, M. W., Bouwmeester, H. J. M., Boukamp, B. A. & Verweij, H. Reactor Flush Time Correction in Relaxation Experiments. *J. Electrochem. Soc.* **148**, J1 (2001).
18. Primdahl, S. & Mogensen, M. Gas diffusion impedance in characterization of solid oxide fuel cell anodes. *J. Electrochem. Soc.* **146**, 2827–2833 (1999).
19. Flura, A. *et al.* Identification and modelling of the oxygen gas diffusion impedance in SOFC porous electrodes: application to $Pr_2NiO_{4+\delta}$. *Electrochim. Acta* **174**, 1030–1040 (2015).
20. Bosanquet, C. H. Wall effects in gas-temperature measurements. (1944).
21. Fuller, E. N. & Giddings, J. C. A Comparison of Methods for Predicting Gaseous Diffusion Coefficients. *Journal of Chromatographic Science* **3**, 222–227 (1965).
22. Knudsen, M. Die Gesetze der Molekularströmung und der inneren Reibungsströmung der Gase durch Röhren. *Ann. Phys.* **333**, 75–130 (1909).
23. Théodon, L., Laurencin, J., Hubert, M., Cloetens, P. & Debayle, J. A stochastic geometrical 3D model for time evolution simulation of microstructures in SOC-electrodes. *Computational Materials Science* **212**, 111568 (2022).
24. Nicollet, C. GLORIA application. *Github* https://github.com/Clement-Nicollet/GLORIA-app.git (2023).
25. Hildebrand, T. & Rüegsegger, P. A new method for the model-independent assessment of thickness in three-dimensional images. *Journal of Microscopy* **185**, 67–75 (1997).
26. Schindelin, J. *et al.* Fiji: an open-source platform for biological-image analysis. *Nat Methods* **9**, 676–682 (2012).
27. Dougherty, B. Local thickness documentation. https://imagej.net/imagej-wiki-static/Local_Thickness.
28. Osterrieth, J. W. M. *et al.* How Reproducible are Surface Areas Calculated from the BET Equation? *Advanced Materials* **34**, 2201502 (2022).
29. Egger, A. & Sitte, W. Enhanced oxygen surface exchange of $La_2NiO_{4+\delta}$ by means of a thin surface layer of silver. *Solid State Ionics* **258**, 30–37 (2014).
30. Tripković, Đ., Küngas, R., Mogensen, M. B. & Hendriksen, P. V. Surface recrystallization – an underestimated phenomenon affecting oxygen exchange activity. *J. Mater. Chem. A* **7**, 11782–11791 (2019).
31. Egger, A., Bucher, E., Yang, M. & Sitte, W. Comparison of oxygen exchange kinetics of the IT-SOFC cathode materials $La_{0.5}Sr_{0.5}CoO_{3-\delta}$ and $La_{0.6}Sr_{0.4}CoO_{3-\delta}$. *Solid State Ionics* **225**, 55–60 (2012).
32. Schaube, M., Merkle, R. & Maier, J. Oxygen exchange kinetics on systematically doped ceria: A pulsed isotope exchange study. *J. Mater. Chem.A* **7**, 21854–21866 (2019).
33. Capdevila-Cortada, M., Vilé, G., Teschner, D., Pérez-Ramírez, J. & López, N. Reactivity descriptors for ceria in catalysis. *Applied Catalysis B: Environmental* **197**, 299–312 (2016).
34. Seo, H. G., Staerz, A., Kim, D. S., LeBeau, J. M. & Tuller, H. L. Tuning Surface Acidity of Mixed Conducting Electrodes: Recovery of Si-Induced Degradation of Oxygen Exchange Rate and Area Specific Resistance. *Advanced Materials* **35**, 2208182 (2023).